White Matter Hyperintensity Associations with Cerebral Blood Flow in Elderly Subjects Stratified by Cerebrovascular Risk

Ahmed A. Bahrani, MS,*,† David K. Powell, PhD,‡ Guoqiang Yu, PhD,* Eleanor S. Johnson, BS,‡ Gregory A. Jicha, MD, PhD,§ and Charles D. Smith, MD*,‡,§

Objective: This study aims to add clarity to the relationship between deep and periventricular brain white matter hyperintensities (WMHs), cerebral blood flow (CBF), and cerebrovascular risk in older persons. *Methods:* Deep white matter hyperintensity (dWMH) and periventricular white matter hyperintensity (pWMH) and regional gray matter (GM) and white matter (WM) blood flow from arterial spin labeling were quantified from magnetic resonance imaging scans of 26 cognitively normal elderly subjects stratified by cerebrovascular disease (CVD) risk. Fluid-attenuated inversion recovery images were acquired using a high-resolution 3-dimensional (3-D) sequence that reduced partial volume effects seen with slice-based techniques. *Results:* dWMHs but not pWMHs were increased in patients at high risk of CVD; pWMHs but not dWMHs were associated with decreased regional cortical (GM) blood flow. We also found that blood flow in WM is decreased in regions of both pWMH and dWMH, with a greater degree of decrease in pWMH areas. *Conclusions:* WMHs are usefully divided into dWMH and pWMH regions because they demonstrate differential effects. 3-D regional WMH volume is a potentially valuable marker for CVD based on associations with cortical CBF and WM CBF. **Key Words:** White matter hyperintensities—small-vessel disease—cerebral blood flow—arterial spin-labeling image—segmentation—fluid-attenuated inversion recovery—vascular risk.

From the *Department of Biomedical Engineering, School of Engineering, University of Kentucky, Lexington, Kentucky; †Department of Biomedical Engineering, AL-Khwarizmi College of Engineering, University of Baghdad, Baghdad, Iraq; ‡Magnetic Resonance Imaging and Spectroscopy Center (MRISC), University of Kentucky, Lexington, Kentucky; and §Department of Neurology, University of Kentucky Medical College, Lexington, Kentucky.

Received June 7, 2016; accepted October 19, 2016.

Grant support: This study was supported by a pilot award (G.Y.) from the National Institutes of Health (NIH) P30 #AG028383 and a grant-in-aid (G.Y.) from the American Heart Association (AHA) #16GRNT30820006.

Address correspondence to Charles D. Smith, MD, Magnetic Resonance Imaging and Spectroscopy Center (MRISC), Room 62, MRISC (Davis-Mills) Building Chandler Medical Center, 740 South Limestone Street, Lexington, KY 40536-0098. E-mail: csmith@mri.uky.edu.

1052-3057/$ - see front matter

http://dx.doi.org/10.1016/j.jstrokecerebrovasdis.2016.10.017

Introduction

Cerebrovascular disease (CVD) is a common medical morbidity in the United States, with high rates of disability through stroke and dementia.[1,2] Detection and characterization of existing CVD, therefore, remain an important medical issue. An understudied aspect of CVD is the relationship between cerebral blood flow (CBF) and white matter hyperintensities (WMHs[3,4]). WMHs are periventricular and deep regions of abnormal signal commonly seen on magnetic resonance imaging (MRI) scans of elderly and high vascular risk patients.[5,6] It has been found that WMHs embody an ischemic component with functional consequences including cognitive decline and dementia, but due to the underlying complexity of these lesions, a full formulation of their significance has not been achieved.[7,8] In the present study, we analyzed the relationship between WMH and CBF in subjects stratified by cerebrovascular risk. The aim of the present study was to find relationships between WMH, CBF, and CVD risk, expecting that WMH would increase with increased CVD risk and with decreased CBF.

Materials and Methods

Subjects

Twenty-six healthy subjects were recruited by the Center for Clinical and Translational Science and the Sanders-Brown Center on Aging at the University of Kentucky. Written consent was obtained from each individual before participation according to an approved protocol from the Institutional Review Board at the University of Kentucky.

A CVD risk score, based on Framingham risk estimation modified for stroke prediction,[9] was assigned to each patient by study neurologists. The Framingham study risk score is based on several parameters, for example, gender, age, history of diabetes, blood pressure, smoking history, and cholesterol level, and is used to predict CVD over 10 years for each subject. The Framingham scoring scale range is 1-30 points.

Subjects were divided, based on their risk score, into 2 groups: high risk (n = 12) and low risk (n = 14) for CVD, based on a cutoff of 15 points. Image analysis was blind to age and CVD risk status.

MRI Acquisition

A Siemens 3T TIM Trio MRI scanner (Siemens Healthcare, Erlangen, Germany) at the University of Kentucky Magnetic Resonance Imaging and Spectroscopy Center equipped with a 32-channel head coil was used to scan subjects. The acquisition sequences were (1) T1-weighted magnetization-prepared rapid-acquisition gradient echo (MP-RAGE): echo time (TE) 2.3 ms, repetition time (TR) 2530 ms, inversion recovery time (IR) 1100 ms, flip angle 7°, $1 \times 1 \times 1$ mm resolution full-brain coverage; (2) fluid-attenuated inversion recovery (FLAIR): TE 388 ms, TR 6000 ms, IR 2200 ms, 3-dimensional (3-D) $1 \times 1 \times 1$ mm with no gap between slices; and (3) pulsed arterial spin labeling: TE 12 ms, TR 3400 ms, IR1 700 ms, IR2 1900 ms, $4 \times 4 \times 4$ mm resolution with 1-mm gap between slices, and full-brain coverage excluding the cerebellum.

Image Processing

MRI image processing used semiautomated methods to quantitate regional WMH volume and CBF flow values. These methods are summarized in Figure 1. Two MP-RAGE images were registered and averaged to increase the signal-to-noise ratio. Scalp and bone tissue were stripped using the FSL FMRIB software library (FSL v5.0.8) Brain Extraction Tool (http://fsl.fmrib.ox.ac.uk/fsl/fslwiki/BET).

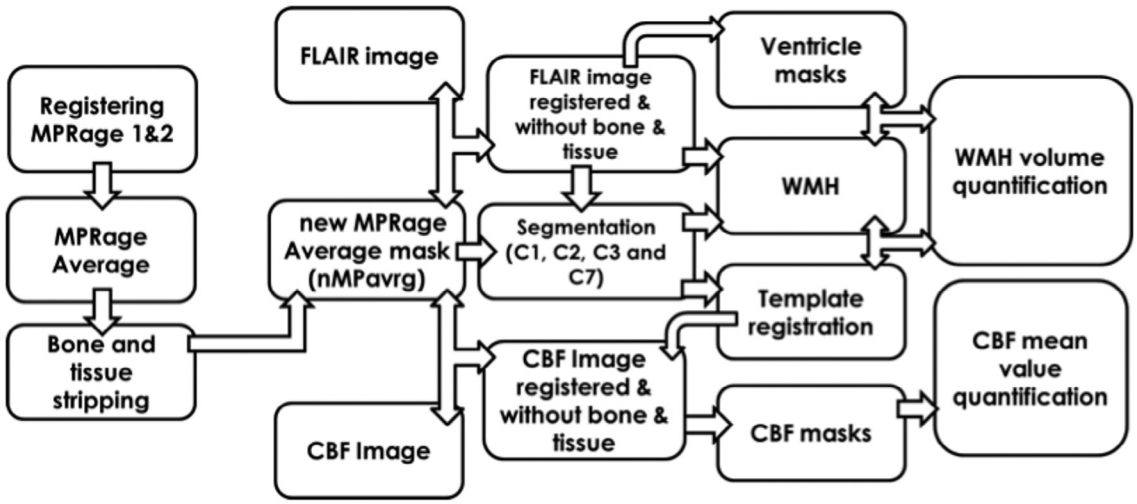

Figure 1. *Diagrammatic overview of the processing workflow for quantitating WMH and cerebral blood flow using FLAIR and arterial spin-labeling images. Segments: C1: gray matter; C2: WM tissue class 1; C3: cerebrospinal fluid; C7: WM tissue class 2. Abbreviations: FLAIR, fluid-attenuated inversion recovery; MP-RAGE, magnetization-prepared rapid-acquisition gradient echo; WM, white matter; WMH, white matter hyperintensity.*

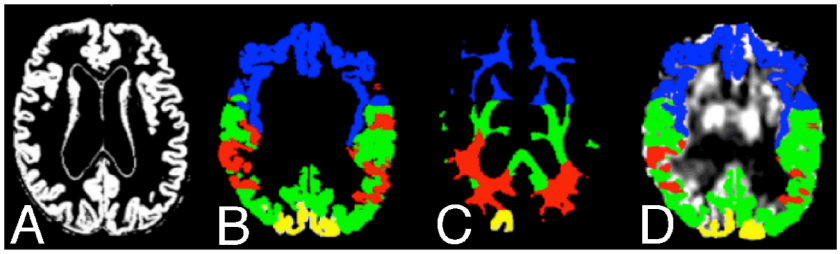

Figure 2. *(A) Native-space GM segmented image. (B and C) International Consortium for Brain Mapping template masks of white matter and GM transferred to the standard space of the subject (compare with A). (D) GM template masks applied to the registered arterial spin-labeling image. Abbreviation: GM, gray matter.*

Slice-by-slice cleanup of unwanted tissue was performed using the Medical Image Processing Analysis and Visualization (MIPAV v7.2.0) application (http://mipav.cit.nih.gov). The stripped brain image was converted to a mask by thresholding (brain mask). FLAIR and pulsed arterial spin-labeling images were registered to the image in SPM12 (http://www.fil.ion.ucl.ac.uk/spm) and stripped of extraneous tissue using the brain mask.

Multimodal segmentation was performed on masked, FLAIR, and ASL brain images in the SPM12 unified regime to create separate native-space images representing gray matter (GM; Fig 2, A), white matter (WM), and cerebrospinal fluid (CSF) using an in-house segmentation template created from 145 images of normal subjects. WM was modeled as 2 separate tissue classes to represent variations due to WM intensities.[10] The International Consortium for Brain Mapping (ICBM) atlas reference was registered to the segmentation template, and atlas regions were combined to create masks representing the frontal, temporal, parietal, and occipital brain regions for both GM (Fig 2, B) and WM (Fig 2, C).

CBF Quantification

The ICBM lobar masks were registered to each subject's native-space ASL image using the inverse transform generated during segmentation. Median CBF values were extracted from each GM template region (Fig 2, D).

WMH Quantification

The 2 WM segmentation images (Fig 3, A,B) were summed (Fig 3, C) and converted to a binary WM mask in native space (Fig 3, D). In a few instances, WM voxels were misclassified in an extraneous tissue segment, likely due to partial volume effects; in these cases, these voxels were added to the 2 WM segments before binary conversion. The unitary WM mask isolated WM in the FLAIR image (Fig 3, E) by multiplication (Fig 3, F). The Gaussian fit to the histogram of WM voxels was used to set the threshold for WMH (Fig 3, G), as the mean plus $3 \times SD$, corresponding to a P value of .01. The individual threshold values were applied to each FLAIR image. The FLAIR

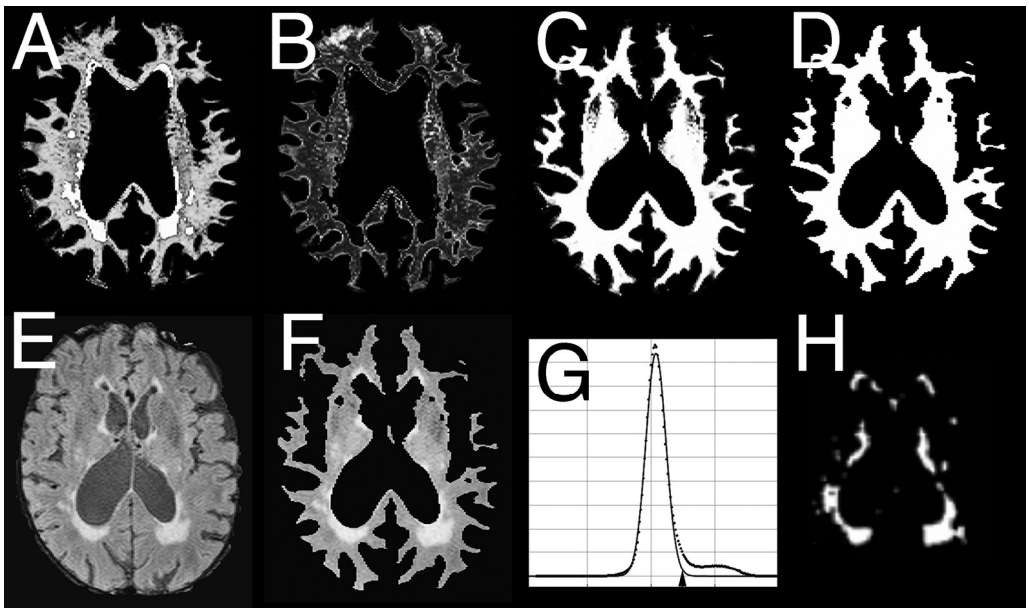

Figure 3. *Sequential steps of the segmentation process to quantitate WMH. (A and B) Segmented images representing 2 tissue classes of WM; (C) total WM (A + B); (D) WM mask from thresholding of D; (E) FLAIR image; (F) FLAIR image masked by D (FLAIR, WM voxels); (G) histogram of E showing Gaussian fit and threshold of 3.0 standard deviation (arrowhead); (H) WMH image obtained by applying threshold to F. Abbreviations: FLAIR, fluid-attenuated inversion recovery; WM, white matter; WMH, white matter hyperintensity.*

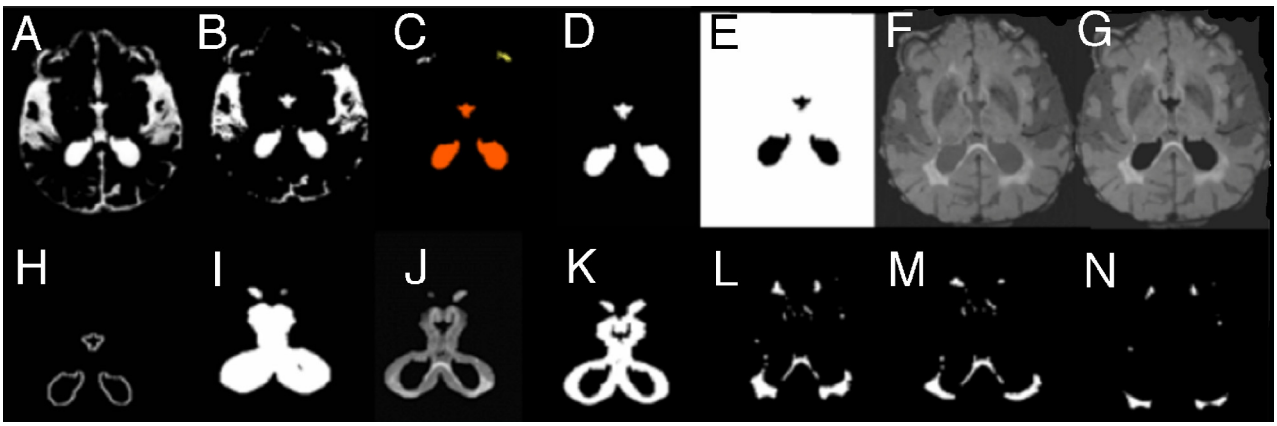

Figure 4. *Sequential steps in obtaining deep WM and periventricular WM binary masks. (A) CSF isolated from other tissues (B) Binarized CSF. (C) Ventricular CSF cluster identified (D) Ventricular tissue voxels. (E) Reversing the intensity of D and multiplying by fluid-attenuated inversion recovery image (F) to remove the CSF (G). (H) The edge of D that is dilated by 5 × 5 × 5 voxels (I). I and G are multiplied to obtain the periventricular tissue (J), which is converted to a binary image (K). (L) WMH image; multiply by K once and the reverse intensity of K once to obtain periventricular WMH and deep WMH, respectively (M and N). Abbreviations: CSF, cerebrospinal fluid; WM, white matter; WMH, white matter hyperintensity.*

image was then Gaussian filtered (1 mm) to remove noise, creating a WMH image for each subject (Fig 3, H).

A final quality-control procedure used a high-contrast display of the FLAIR image at the Gaussian-fit mean center and window value of 10 × SD, side by side with the WMH image, comparing slice by slice for correspondence between isolated WMH and FLAIR hyperintensities. Manual editing of extraneous pixels due to pulsation and flow artifacts was needed occasionally, resulting in the final WMH image (Fig 3, H), quantitated by calculating the total voxel and the total WMH voxel volume.[10]

Voxels in the WMH image were divided into pWMH and dWMH using the following method designed to produce a reproducible and consistent definition of pWMH and dWMH: (1) the CSF segment (Fig 4, A) was used to generate a mask by thresholding at .33 (Fig 4, B); connected voxels were morphologically identified as belonging to ventricles (Fig 4, C) and isolated (Fig 4, D); the ventricular volume was intensity-inverted (Fig 4, E) and multiplied by the FLAIR image (Fig 4, F) to exclude the CSF (Fig 4, G); (2) the border of the ventricular mask was morphologically identified (Fig 4, H) and dilated (5^3 voxels; Fig 4, I), then multiplied by the CSF-excluded FLAIR image to identify periventricular tissue (Fig 4, J); 10% of the mean value from periventricular tissue voxel histogram was set as minimum threshold level to obtain the periventricular binary mask (Fig 4, K); and (3) this mask was multiplied by the total WMH mask (Fig 4, L; cf. Fig 3, H) to obtain the pWMH (Fig 4, M), and the negative of this periventricular binary mask was multiplied by the total WMH mask to obtain the dWMH (Fig 4, N).

Statistical Methods

Multivariate analysis of variance models used log-transformed measured WMH volumes as repeated independent variables because of their typical skewed distributions (JMP v9; SAS Institute, Cary, NC). The dependent variables were the risk group (high versus low vascular risk) and the total intracranial volume (TIV) to control for head size. Post hoc contrasts of dWMH and pWMH versus risk group relationships were performed. A similar model was used for ASL CBF in 3 defined WM regions: 2 regions contained either dWMH or pWMH, and 1 region had no WMH. Age, risk group, and TIV were used as covariates in this model.

To test relationships between dWMH and pWMH, a standard least squares model was constructed with log dWMH as the dependent variable, and the risk group was nested within log pWMH as the independent variable, with TIV as control for head size. A P value of .05 was considered significant; a P value less than .10 was marginally significant.

Results

The 26 subjects had a mean age of 77.8 ± 6.8 years (range 66-88). There were 23 females (mean age 77.8 ± 6.9) and 3 males (mean age 77.0 ± 7.9).

There was a significant difference in age between risk groups: the low-risk group had a mean age of 72.7 ± 4.2 and the high-risk group had a mean age of 83 ± 4.6 ($P < .0001$).

WMHs

Total WMH volume positively correlated with independent visual ratings using the Longstreth scale,[11] confirming that volumes correspond to what a trained neurologist interprets as WMH (Fig 5, A). There was a significant correlation between pWMH and dWMH in the regression model, but the relationship between pWMH and dWMH was different for high- and low-risk subjects: the slope of regression was higher in the high-risk

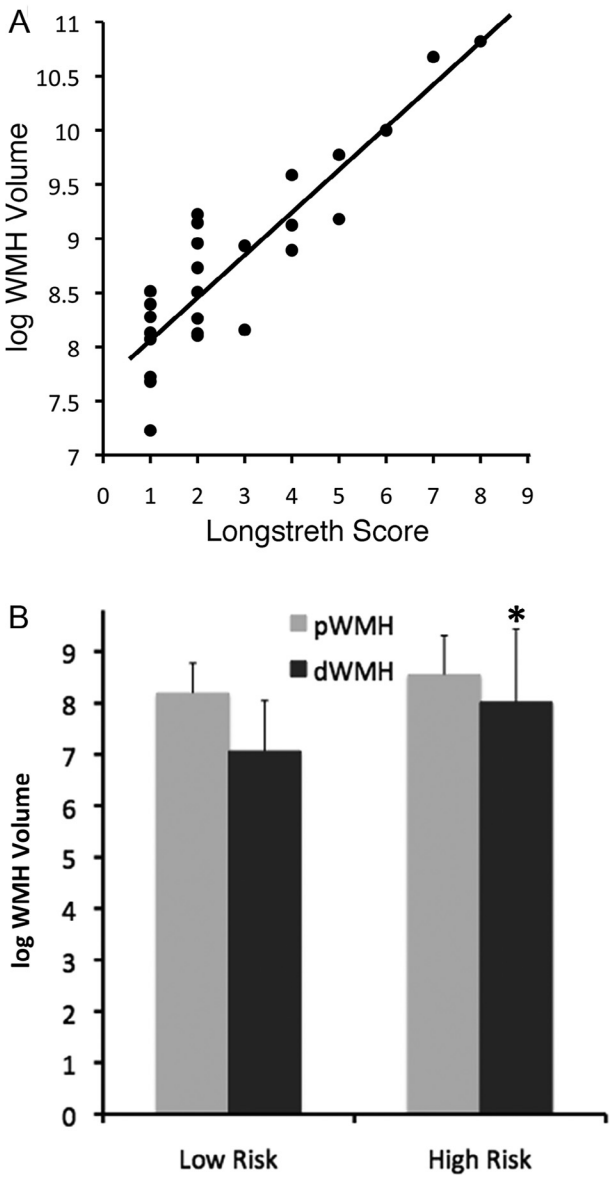

Figure 5. *(A) Linear regression of Longstreth visual rating scale (0-9) for all patients on log WMH total volume, demonstrating the face validity of the WMH volume measurement (adjusted* $r^2 = .88$, $P < .0001$*), (B) log WMH volume in low- and high-risk groups; overall volume is higher in high-risk patients (*$P = .02$*), but only the dWMH volume is significant (**$P = .04$*, error bars = standard deviation). Abbreviations: dWMH, deep white matter hyperintensity; pWMH, periventricular white matter hyperintensity; WMH, white matter hyperintensity.*

group (standard error of the mean = 1.26 ± .22, $t = 5.5$, $P < .0001$) than in the low-risk group (standard error of the mean = .86 ± .34, $t = 2.5$, $P = .02$). The mean dWMH volume was higher in the high-risk group than in the low risk group ($t = 2.3$, $P = .03$; Fig 5, B).

Multivariate analysis of variance confirmed that WMH volume was higher in the high-risk group ($F = 5.8$, $P = .02$). Further analysis demonstrates that dWMH volume was higher in the high-risk group ($t = 2.2$, $P = .04$), but pWMH volume was not significantly different ($t = 1.0$, $P = .34$) between groups.

Age correlated with total WMH ($P = .04$) and dWMH ($P = .03$) but not pWMH volume ($P = .10$). There was a strong correlation seen between age and risk score ($r^2 = .56$, $P < .0001$).

CBF

There were no differences in global or in regional cortical GM CBF between risk groups. There was no association between CBF and age. We analyzed associations between WMH volume and regional CBF. Results are shown in Table 1. Correlations were significant between parietal WMH volume and posterior frontal, parietal, temporal, and occipital CBF, and marginally significant with total CBF. Occipital pWMH volume was significantly correlated with CBF in the medial temporal GM (Table 1).

Average WM CBF was calculated for 3 WM regions containing dWMH, pWMH, or either lesion ($F = 53.5$, $P < .0001$; Fig 6). Age, risk group, and TIV did not significantly affect CBF. Post hoc paired comparisons showed a significantly decreased CBF in the dWMH ($t = 5.7$, $P < .001$) and pWMH ($t = 11.0$, $P < .0001$) regions compared to normal-appearing WM. CBF in the pWMH was less than that in dWMH areas ($t = 3.1$, $P = .003$).

Discussion

The aim of the present study was to find relationships between WMH, CBF, and CVD risk in elderly patients. CVD risk was assessed by the Framingham CVD stroke risk score assigned to each patient. Fourteen subjects with low risk were compared to 12 subjects with

Table 1. *Spearman rank correlations for the pWMH and CBF for different brain regions*

WMH	Total	Frontal (ant)	Frontal (post)	Occipital	Parietal	Temporal	Temporal (medial)
Total	−.28 (.15)	−.16 (.41)	−.33 (.09)	−.37 (.06)	−.37 (.06)	−.37 (.06)	−.31 (.11)
Frontal	−.16 (.41)	−.16 (.41)	−.24 (.23)	−.21 (.29)	−.17 (.37)	−.23 (.23)	−.25 (.20)
Occipital	−.06 (.73)	.13 (.50)	−.006 (.97)	−.08 (.66)	−.07 (.72)	−.25 (.19)	−.42 (.03)*
Parietal	−.34 (.08)	−.28 (.15)	−.39 (.04)*	−.39 (.04)*	−.44 (.02)*	−.38 (.05)*	−.30 (.13)
Temporal	−.13 (.49)	.004 (.98)	−.09 (.63)	−.23 (.24)	−.18 (.36)	−.23 (.24)	−.29 (.14)

Abbreviations: CBF, cerebral blood flow; dWMH, deep white matter hyperintensity; pWMH, periventricular white matter hyperintensity.
There were no significant correlations between dWMH or total WMH volume with CBF.
*Denotes significant *P* value.

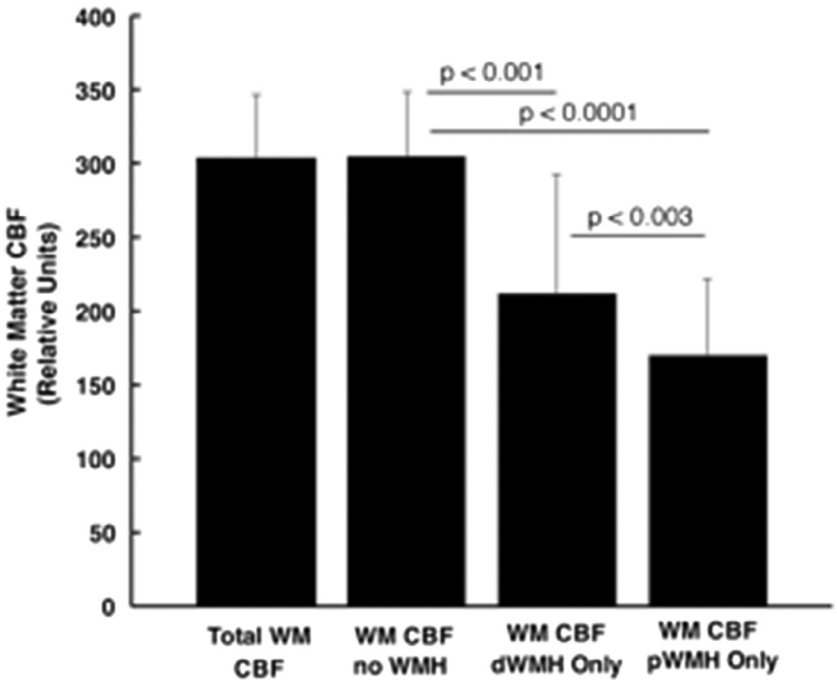

Figure 6. *Arterial spin-labeling blood flow in the WM (left to right): total WM including WMH, total WM but excluding WMH, dWMH regions, and pWMH regions. Paired comparisons are significantly different as shown. Lowest CBF is in the pWMH regions. Bar height: mean CBF; error bars: standard deviation. Abbreviations: CBF, cerebral blood flow; dWMH, deep white matter hyperintensity; pWMH, periventricular white matter hyperintensity; WM, white matter; WMH, white matter hyperintensity.*

high risk. We used a 3-D FLAIR WMH imaging technique that improved resolution and registration, and reduced partial volume effects compared to slice-based techniques. The main findings are that dWMHs but not pWMHs are increased in high-risk patients, and that pWMHs but not dWMHs are associated with decreased regional cortical (GM) blood flow. We also found that blood flow in WM is decreased in regions of both pWMH and dWMH, with a greater degree of decrease in pWMH areas.

The underlying origin of WMH remains controversial, perhaps because different mechanisms responsible for their appearance and pathologies can be found at autopsy that so far are not distinguishable using current MRI methods.[2,7,12-18] The strongest and most consistent associations with WMH are age and certain cerebrovascular risk factors including diabetes, hypertension, hypercholesterolemia, and cigarette smoking.[8,9,19-26] These factors are included in vascular risk measures such as the Framingham score used in the present study. A genetic component may be involved in cases where evidence of CVD is lacking.[27-31]

Age associations with WMH are likely explained by the accumulation of vascular disease over time together with other changes in cerebral WM that may be unrelated to small-vessel CVD per se, such as cerebral amyloid angiopathy or Alzheimer's disease-related changes.[32,33] Nonetheless, WMHs are taken with much supporting evidence to represent a marker of classical small-vessel CVD in WM. Small-vessel CVD is increasingly recognized as an important pathological contributor to clinical decline in our aging U.S. population, showing strong associations with both gait disorders and vascular dementia.[34-36] Vascular dementia can occur as a pure form, or often together with more common dementias including Alzheimer's disease (where it is termed mixed vascular dementia).[37]

We divided WMH into dWMH and pWMH for several reasons.[10,38-42] First, the WM tracts adjacent to the ventricles encompassed by pWMHs are limbic (cingulum) and motor (corticospinal and related tracts), whereas dWMHs are more likely to involve long association tracts and thus long-range inter-regional connectivity. The possibility that clinical correlates of dWMH and pWMH may be different is also supported by the association of dWMH but not pWMH with vascular dementia.[10,43] Finally, the small-vessel circulation in WM may be different between deep and periventricular zones, with a greater vulnerability of the periventricular region to large-vessel disease.[44] This is consistent with our finding that low cortical CBF is associated with greater pWMH.

We found that the relationship between pWMH and dWMH was different depending on the risk group: the increase in dWMH per given change in pWMH was higher in the high-risk group, even though pWMH volume was the same. This finding suggests that vascular risk factors are associated with more widespread small-vessel disease in WM, whether directly or indirectly via large-vessel flow compromise. Other evidence of small-vessel disease in our data was decreased WM CBF in both dWMH and pWMH regions. However, these differences were not related to age or to CVD risk status.

There are several caveats to the interpretation of our data. The first is the association between age and risk status in our patients. Age is strongly associated with CVD, but there may be other independent effects of age on WMH

that we are not able to discern in our analysis. Better selection of subjects and larger recruitment would have helped overcome this limitation. Another caution is the relatively low proportion of patients with high grades of WMH. We were able to offset this problem by normalizing distributions of WMH and using nonparametric correlations for CBF, still achieving significant results, but these findings should be confirmed in future studies. Additional methodological analysis considerations include our planned use of a 3-D ASL acquisition for better comparison with 3-D WMH volumes.

Conclusions

We find evidence that WMHs are usefully divided into dWMH and pWMH regions because they demonstrate differential associations with CVD and demographic risk factors. 3-D WMH volume is a potentially valuable marker for CVD that is able to differentiate associations of pWMH and dWMH with risk factor profiles as well as cortical CBF and WM CBF. Further studies using such methods in distinct and larger cohorts are needed to conform and extend the present findings.

Acknowledgments: We acknowledge the support from The Higher Committee for Education Development in Iraq, the assistance from Weikai Kong, Yu Shang, Chong Huang, and Abner Rayapati, and the help we received from the University of Kentucky Alzheimer's Disease Center (ADC), particularly from Dr. Fred Schmitt of the ADC.

References

1. Go AS, Mozaffarian D, Roger VL, et al. Heart disease and stroke statistics—2014 update: a report from the American Heart Association. Circulation 2014;129:e28-e292.
2. Jellinger KA. The pathology of ischemic-vascular dementia: an update. J Neurol Sci 2002;203-204:153-157.
3. Brickman AM, Zahra A, Muraskin J, et al. Reduction in cerebral blood flow in areas appearing as white matter hyperintensities on magnetic resonance imaging. Psychiatry Res 2009;172:117-120.
4. Bastos-Leite AJ, Kuijer JP, Rombouts SA, et al. Cerebral blood flow by using pulsed arterial spin-labeling in elderly subjects with white matter hyperintensities. AJNR Am J Neuroradiol 2008;29:1296-1301.
5. Gootjes L, Teipel SJ, Zebuhr Y, et al. Regional distribution of white matter hyperintensities in vascular dementia, Alzheimer's disease and healthy aging. Dement Geriatr Cogn Disord 2004;18:180-188.
6. Debette S, Markus HS. The clinical importance of white matter hyperintensities on brain magnetic resonance imaging: systematic review and meta-analysis. BMJ 2010;341:c3666.
7. Raman MR, Preboske GM, Przybelski SA, et al. Antemortem MRI findings associated with microinfarcts at autopsy. Neurology 2014;82:1951-1958.
8. Wardlaw JM, Allerhand M, Doubal FN, et al. Vascular risk factors, large-artery atheroma, and brain white matter hyperintensities. Neurology 2014;82:1331-1338.
9. D'Agostino RB, Wolf PA, Belanger AJ, et al. Stroke risk profile: adjustment for antihypertensive medication. The Framingham Study. Stroke 1994;25:40-43.
10. Smith CD, Johnson ES, Van Eldik LJ, et al. Peripheral (deep) but not periventricular MRI white matter hyperintensities are increased in clinical vascular dementia compared to Alzheimer's disease. Brain Behav 2016;6:e00438.
11. Longstreth WT Jr, Manolio TA, Arnold A, et al. Clinical correlates of white matter findings on cranial magnetic resonance imaging of 3301 elderly people. The Cardiovascular Health Study. Stroke 1996;27:1274-1282.
12. Erten-Lyons D, Woltjer R, Kaye J, et al. Neuropathologic basis of white matter hyperintensity accumulation with advanced age. Neurology 2013;81:977-983.
13. Gouw AA, Seewann A, van der Flier WM, et al. Heterogeneity of small vessel disease: a systematic review of MRI and histopathology correlations. J Neurol Neurosurg Psychiatry 2011;82:126-135.
14. Hooshmand B, Polvikoski T, Kivipelto M, et al. Plasma homocysteine, Alzheimer and cerebrovascular pathology: a population-based autopsy study. Brain 2013;136:2707-2716.
15. Jagust WJ, Zheng L, Harvey DJ, et al. Neuropathological basis of magnetic resonance images in aging and dementia. Ann Neurol 2008;63:72-80.
16. Kaur B, Himali JJ, Seshadri S, et al. Association between neuropathology and brain volume in the Framingham Heart Study. Alzheimer Dis Assoc Disord 2014;28:219-225.
17. Smith CD, Snowdon DA, Wang H, et al. White matter volumes and periventricular white matter hyperintensities in aging and dementia. Neurology 2000;54:838-842.
18. Smith CD, Snowdon D, Markesbery WR. Periventricular white matter hyperintensities on MRI: correlation with neuropathologic findings. J Neuroimaging 2000;10:13-16.
19. Abraham HM, Wolfson L, Moscufo N, et al. Cardiovascular risk factors and small vessel disease of the brain: blood pressure, white matter lesions, and functional decline in older persons. J Cereb Blood Flow Metab 2015;36:132-142.
20. Gattringer T, Enzinger C, Ropele S, et al. Vascular risk factors, white matter hyperintensities and hippocampal volume in normal elderly individuals. Dement Geriatr Cogn Disord 2012;33:29-34.
21. Jeerakathil T, Wolf PA, Beiser A, et al. Stroke risk profile predicts white matter hyperintensity volume: the Framingham Study. Stroke 2004;35:1857-1861.
22. Miwa K, Tanaka M, Okazaki S, et al. Multiple or mixed cerebral microbleeds and dementia in patients with vascular risk factors. Neurology 2014;83:646-653.
23. Rostrup E, Gouw AA, Vrenken H, et al. The spatial distribution of age-related white matter changes as a function of vascular risk factors—results from the LADIS study. Neuroimage 2012;60:1597-1607.
24. Vuorinen M, Spulber G, Damangir S, et al. Midlife CAIDE dementia risk score and dementia-related brain changes up to 30 years later on magnetic resonance imaging. J Alzheimers Dis 2015;44:93-101.
25. Wang R, Fratiglioni L, Laukka EJ, et al. Effects of vascular risk factors and APOE epsilon4 on white matter integrity and cognitive decline. Neurology 2015;84:1128-1135.
26. Wang R, Fratiglioni L, Laveskog A, et al. Do cardiovascular risk factors explain the link between white matter hyperintensities and brain volumes in old age? A population-based study. Eur J Neurol 2014;21:1076-1082.

27. Adib-Samii P, Devan W, Traylor M, et al. Genetic architecture of white matter hyperintensities differs in hypertensive and nonhypertensive ischemic stroke. Stroke 2015;46:348-353.
28. Adib-Samii P, Rost N, Traylor M, et al. 17q25 Locus is associated with white matter hyperintensity volume in ischemic stroke, but not with lacunar stroke status. Stroke 2013;44:1609-1615.
29. Carmelli D, DeCarli C, Swan GE, et al. Evidence for genetic variance in white matter hyperintensity volume in normal elderly male twins. Stroke 1998;29:1177-1181.
30. Haffner C, Malik R, Dichgans M. Genetic factors in cerebral small vessel disease and their impact on stroke and dementia. J Cereb Blood Flow Metab 2016;36:158-171.
31. Lin Q, Huang WQ, Tzeng CM. Genetic associations of leukoaraiosis indicate pathophysiological mechanisms in white matter lesions etiology. Rev Neurosci 2015;26:343-358.
32. Gurol ME, Viswanathan A, Gidicsin C, et al. Cerebral amyloid angiopathy burden associated with leukoaraiosis: a positron emission tomography/magnetic resonance imaging study. Ann Neurol 2013;73:529-536.
33. Lo RY, Jagust WJ. Vascular burden and Alzheimer disease pathologic progression. Neurology 2012;79:1349-1355.
34. Kalaria RN, Erkinjuntti T. Small vessel disease and subcortical vascular dementia. J Clin Neurol 2006;2:1-11.
35. Baezner H, Blahak C, Poggesi A, et al. Association of gait and balance disorders with age-related white matter changes: the LADIS study. Neurology 2008;70:935-942.
36. van Norden AG, de Laat KF, Gons RA, et al. Causes and consequences of cerebral small vessel disease. The RUN DMC study: a prospective cohort study. Study rationale and protocol. BMC Neurol 2011;11:29.
37. Kalaria RN. Vascular basis for brain degeneration: faltering controls and risk factors for dementia. Nutr Rev 2010;68(Suppl 2):S74-S87.
38. Blahak C, Baezner H, Pantoni L, et al. Deep frontal and periventricular age related white matter changes but not basal ganglia and infratentorial hyperintensities are associated with falls: cross sectional results from the LADIS study. J Neurol Neurosurg Psychiatry 2009;80:608-613.
39. Kee Hyung P, Lee JY, Na DL, et al. Different associations of periventricular and deep white matter lesions with cognition, neuropsychiatric symptoms, and daily activities in dementia. J Geriatr Psychiatry Neurol 2011;24:84-90.
40. Krishnan MS, O'Brien JT, Firbank MJ, et al. Relationship between periventricular and deep white matter lesions and depressive symptoms in older people. The LADIS Study. Int J Geriatr Psychiatry 2006;21:983-989.
41. Noh Y, Lee Y, Seo SW, et al. A new classification system for ischemia using a combination of deep and periventricular white matter hyperintensities. J Stroke Cerebrovasc Dis 2014;23:636-642.
42. Soriano-Raya JJ, Miralbell J, Lopez-Cancio E, et al. Deep versus periventricular white matter lesions and cognitive function in a community sample of middle-aged participants. J Int Neuropsychol Soc 2012;18:874-885.
43. Spilt A, Goekoop R, Westendorp RG, et al. Not all age-related white matter hyperintensities are the same: a magnetization transfer imaging study. AJNR Am J Neuroradiol 2006;27:1964-1968.
44. De Reuck J. The human periventricular arterial blood supply and the anatomy of cerebral infarctions. Eur Neurol 1971;5:321-334.